J Syst Sci Complex (2024) 37(2): 581–608

Three-Rigid-Body-Particle Modeling and Optimization of Trajectory and Posture for Alpine Skiing*

ZHANG Yijia · FEI Qing · YAO Xiaolan · SUN Jian · ZHANG Yanjun · CHEN Zhen

DOI: 10.1007/s11424-024-3021-7
Received: 20 January 2023 / Revised: 26 April 2023

Abstract This paper presents a new study on modeling and optimization of trajectory and posture for the super-giant (SG) slalom of alpine skiing. It is the first time that a Three-Rigid-Body-Particle model based on rigorous derivations and stability analysis is established to represent skiers trajectory and posture characteristics, as it is more accurate than the single-rigid-body model which is commonly used in existing studies. In addition, the Radau pseudospectral method is applied to solve the trajectory and posture optimization problem in order to obtain better skiing trajectory, skiing posture, and some key kinematic parameters of skiers. Moreover, this paper analyzes the effects of different body types, minimum turning radii, and flexor and extensor strength of knees and hip joint on skiing performance. Finally, based on the findings of the study, some advice about how to improve the performance of the SG slalom in view of science and technology is given to skiers and coaches for reference.

Keywords Alpine skiing modeling, posture optimization, Three-Rigid-Body-Particle model, trajectory optimization.

1 Introduction

The traditional training guidance mode relying on the experience of coaches no longer meets the requirements of competitive sports. More sports need to exploit scientific and technological approaches to support sports development. The complex systems approach proposes a deep change in sport science and provides more precise and accurate guidance for the selection and training of athletes[1]. The role of technology in competitive sports is becoming more prominent, and athletes increasingly rely on scientific and personalized training plans.

ZHANG Yijia · FEI Qing (Corresponding author) · YAO Xiaolan · SUN Jian · ZHANG Yanjun · CHEN Zhen *School of Automation, Beijing Institute of Technology, Beijing* 100081, *China.* Email: 15601259677@163.com; feiqing@bit.edu.cn; yaoxiaolan@bit.edu.cn; sunjian@bit.edu.cn; yanjun@bit.edu.cn; chenzhen76@bit.edu.cn.
*This research was supported in part by the Key Technology Research and Demonstration of National Scientific Training Base Construction of China under Grant No. 2018YFF0300800, in part by the National Natural Science Foundation of China under Grant No. 62173323, and in part by Beijing Institute of Technology Research Fund Program for Young Scholars.
◇*This paper was recommended for publication by Editor HE Wei.*

Sport is a complex and changeable system. In this sense, the complex systems approach provides a perspective of the foremost interest when it comes to analyze sports[2]. It has been widely verified in the literature that the complex systems approach can significantly improve athletic performance. For instance, the reference [3] addressed the correlation between driving distance and isokinetic strength in golf and proposed an optimized training scheme aimed at improving the performance of golfers was proposed. The reference [4] analyzed the World Cup Final 2006 between France and Italy by means of relative phase to understand the complexity of soccer. Some skating techniques for the straights based on the optimization of a simulation model was proposed in [5]. In this paper, we focus on how to improve the performance of the super-giant (SG) slalom of alpine skiing in view of science and technology. The modeling and optimization of alpine skiing has been widely addressed in the literature. The reference [6] described the entire ski system as a particle model and optimized the skiing trajectory. In [7], the movement of the "skier-ski" system on the slope was regarded as the movement of a particle in the inertial system. To describe the skiing system more accurately, inverted pendulum models were addressed to simulate the slalom of alpine skiing in [8–10]. A pole model was proposed in the reference [11] to describe the ski-skier system as a particle connected with a weightless rod. There is also some research on the optimization of skiing. A program is developed for numerical simulation and optimization of the pacing strategy in cross-country ski racing in [12]. The reference [13] optimized the original inrun system in ski jumping and improved the level of competition.

Although the modeling and optimization of alpine skiing have been widely addressed, there are still two open issues.

1) The existing skiing models, including the particle model, inverted pendulum model, and pole model, can describe the trajectory. However, it is still an open research question about how to establish a model that can have more degrees of freedom and describe the trajectory-and-posture simultaneously.

2) The existing references mainly addressed how to optimize the skiing trajectory. However, besides the trajectory, posture and other kinematic parameters are vital in skiing competition. How to simultaneously address all these issues in optimizing the skiing performance is still open for study.

In this paper, we conduct a new study on modeling and optimization of trajectory-and-posture for the SG slalom of alpine skiing. The main contributions of this paper are summarized as follows.

1) A Three-Rigid-Body-Particle (TRBP) model is established to represent the skiers' posture characteristics more accurately than the existing results for the SG slalom of alpine skiing.

2) The alpine skiing trajectory-and-posture optimization problem of the established TRBP model is solved based on the Radau pseudospectral method (RPM). As a result, the optimal skiing trajectory, skiing posture, and some key kinematic parameters of skiers are obtained.

3) The effects of different body types, minimum turning radius, and flexor and extensor strength of knees and hip joint on skiing performance are analyzed. Based on the obtained results, some advice about how to improve the performance of the SG slalom of alpine skiing

in view of science and technology are given to skiers and coaches for reference.

The rest of this paper is organized as follows. Section 2 presents the TRBP model. Section 3 discusses the trajectory-and-posture optimization model of the skiing system. Section 4 shows the simulation study. Section 5 gives the concluding remarks.

2 Model and Description

In this section, we give the alpine skiing model and clarify technical issues to be solved. The notations used in this paper are summarized in Table 1.

Table 1 The notations used in this paper

Notations	Description
x, y	the displacements of m_0 on the OX-axis and OY-axis
β	the slope of the track
m_0, m_1, m_2, m_3	the masses of the particle and rigid bodies 1, 2, 3
l_1, l_2, l_3	lengths of rigid bodies 1, 2, 3
v	the velocity of the skier
v_0, v_1, v_2, v_3	the velocities of m_0, m_1, m_2, m_3 on the $o'y_2$-axis
θ	the tangential angle (angle between v_0 and $o'y_1$-axis)
F_N, F_L	the supporting force of the ground to the human body on the $o'z_2$-axis and the $o'y_2$-axis
F_{P1}	the force of m_1 on skis m_0
$F_{P1'}$	the force of skis m_0 on m_1
F_{P2}	the force of m_2 on m_1
$F_{P2'}$	the force of m_1 on m_2
F_{P3}	the force of m_3 on m_2
$F_{P3'}$	the force of m_2 on m_3
G_{z_20}, G_{z_21}, G_{z_22}, G_{z_23}	the gravity components of m_0, m_1, m_2, m_3 on the $o'z_2$-axis
G_{x_20}, G_{x_21}, G_{x_22}, G_{x_23}	the gravity components of m_0, m_1, m_2, m_3 on the $o'x_2$-axis
F_{C0}, F_{C1}, F_{C2}, F_{C3}	the centripetal forces of m_0, m_1,m_2, m_3 on the $o'x_2$-axis
F_{m_0}, F_{m_1}, F_{m_2}, F_{m_3}	the resultant forces on m_0, m_1, m_2, m_3
r_0, r_1, r_2, r_3	the turning radius of m_0, m_1, m_2, m_3
ω_1, ω_1, ω_3, ω_4	the angular velocities corresponding to φ_1, φ_2, φ_3, φ_4

2.1 Three-Rigid-Body-Particle Model

To facilitate the dynamic analysis of skiing, as shown in Figure 1, we establish three reference coordinate systems. They are the inertial reference coordinate system $OXYZ$ relative to the ground, the fixed reference system $o'x_1y_1z_1$ relative to the multi-rigid-body model, and the non-inertial reference coordinate system $o'x_2y_2z_2$. The origin o' is the geometric center of the skis. For the coordinate system $o'x_1y_1z_1$, $o'x_1$, $o'y_1$, and $o'z_1$ axes are parallel to OX, OY, and

OZ axes, respectively. For the coordinate system $o'x_2y_2z_2$, the direction of the $o'y_2$-axis is that of the skier's velocity, while the direction of $o'x_2$-axis is perpendicular to that of skis' long axis.

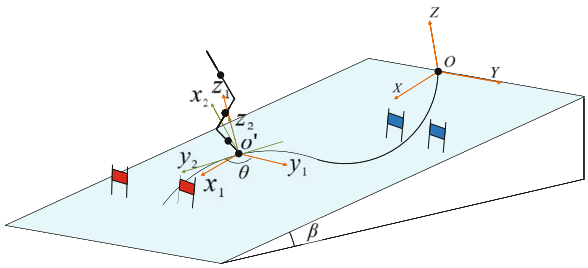

Figure 1 Alpine skiing coordinate system diagram

Considering that the lower legs, the thighs, and the trunk represent the skiers posture characteristics well, as shown in Figure 2, we establish a TRBP model. In this model, the rigid-body-1 represents the lower legs with length l_1 and mass m_1, the rigid-body-2 represents the thighs with length l_2 and mass m_2, and the rigid-body-3 represents the trunk with length l_3 and mass m_3. The centroids of the rigid bodies are located at the geometric center of the rigid bodies. Moreover, the skis are represented as a particle model with mass m_0.

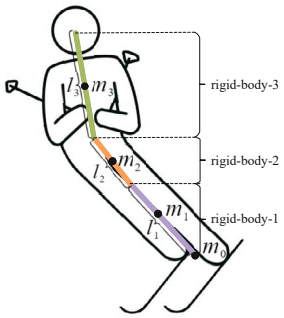

Figure 2 Schematic diagram of TRBP model

The TRBP model established in this paper has seven degrees of freedom. Rigid-body-1 has one degree of freedom that can rotate around o' in the $o'x_2z_2$ plane (the coronal plane of the human body). Rigid-body-2 has one degree of freedom that can rotate around the hinge in the $o'y_2z_2$ plane (the sagittal plane of the human body). Rigid-body-3 is connected to rigid-body-2 by the hinge and has two degrees of freedom that can rotate around the hinge in the $o'x_2z_2$ plane and $o'y_2z_2$ plane. The other three degrees of freedom are the model's displacements x,y and direction of movement θ.

2.2 Equations of Motion

In this paper, the ski slope is assumed to be flat, on which the model skied without skidding. The snow friction coefficient, the drag coefficient and the mass density of the air remain unchanged. The definitions of φ_n, v_n, and r_n $(n = 1, 2, 3, 4)$ are shown in Figure 3. The angle

φ_1 is the inclination angle of the lower legs, φ_2 is the flexion angle of the knees, φ_3 is the inclination angle of the trunk, and φ_4 is the flexion angle of the trunk. During the modeling process, only five forces were considered, namely gravity G, supporting force F_N, snow friction f_r, aerodynamic drag f_a and centripetal force F_C, without external force driving the model.

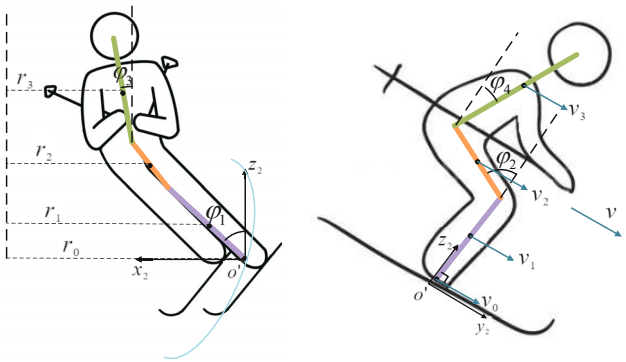

(a) Coronal view (b) Sagittal view

Figure 3 (a) Schematic diagram of TRBP model in the coronal view (the $o'x_2z_2$ plane); (b) Schematic diagram of TRBP model in the sagittal view (the $o'y_2z_2$ plane)

Based on the physical meanings of x, y, v_0, and θ, it yields

$$\begin{cases} \dot{x} = v_0 \sin\theta, \\ \dot{y} = v_0 \cos\theta. \end{cases} \tag{1}$$

Since angular velocity ω_i is the derivative of rotation angle φ_i, then

$$\omega_n = \dot{\varphi}_n, \quad n = 1, 2, 3, 4. \tag{2}$$

From Figure 3(b), comparing the values between v_0, v_1, v_2, and v_3 yields

$$\begin{cases} v_1 - v_0 = 0, \\ v_2 - v_1 = 0.5 l_2 \omega_2 \cos\varphi_2, \\ v_3 - v_2 = 0.5 l_2 \omega_2 \cos\varphi_2 + 0.5 l_3 \omega_4 \cos\varphi_4. \end{cases} \tag{3}$$

Since the skier's velocity, denoted by v, is practically equal to v_0, we get

$$\begin{cases} v_1 = v, \\ v_2 = v + 0.5 l_2 \omega_2 \cos\varphi_2, \\ v_3 = v + l_2 \omega_2 \cos\varphi_2 + 0.5 l_3 \omega_4 \cos\varphi_4. \end{cases} \tag{4}$$

From Figure 3(a), comparing the values between r_0, r_1, r_2, and r_3 yields

$$\begin{cases} r_0 - r_1 = 0.5 l_1 |\sin\varphi_1|, \\ r_1 - r_2 = 0.5 l_1 |\sin\varphi_1| + 0.5 l_2 |\sin\varphi_1|, \\ r_2 - r_3 = 0.5 l_2 |\sin\varphi_1| + 0.5 l_3 |\sin\varphi_3|. \end{cases} \tag{5}$$

Based on the real skiing situation, it can be seen that r_0 and r_i are equal, that is, $r_0 = r_n$, $n = 1, 2, 3$. From the conversion equation of linear velocity and angular velocity, it yields

$$\dot{\theta} = \frac{v_0}{r_0} \operatorname{sgn} \dot{\theta}. \tag{6}$$

With Figures 4–8 to hand, we start to carry out the force analysis of m_0, m_1, m_3, and the overall system.

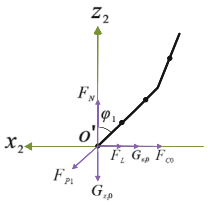

Figure 4 m_0 force analysis

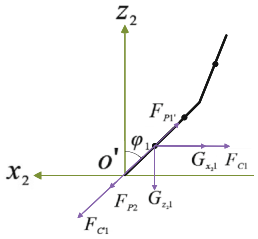

Figure 5 m_1 force analysis

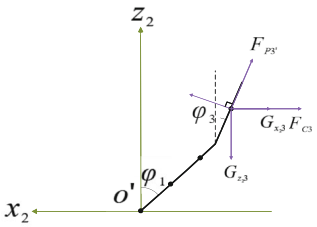

Figure 6 m_3 force analysis

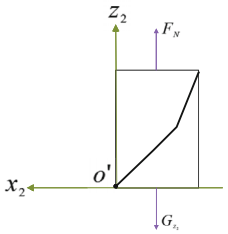

Figure 7 Overall system force analysis (coronal view)

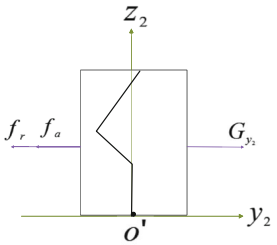

Figure 8 Overall system force analysis (sagittal view)

2.2.1 Force Analysis of m_0

As shown in Figure 4, the forces applied on the $o'z_2$-axis and $o'x_2$-axis are

$$\begin{cases} F_N = F_{P1} \cos \varphi_1 + G_{z_2 0}, \\ F_{C0} = F_L + G_{x_2 0} - F_{P1} \sin \varphi_1, \end{cases} \tag{7}$$

where

$$\begin{cases} G_{z_20} = m_0 g \cos\beta, \\ F_{C0} = -m_0 \dfrac{{v_0}^2}{r_0} \operatorname{sgn}\dot{\theta}, \\ G_{x_20} = m_0 g \sin\beta \cos\theta. \end{cases} \tag{8}$$

2.2.2 Force Analysis of m_1

As shown in Figure 5, the forces applied on the $o'z_2$-axis and $o'x_2$-axis are

$$\begin{cases} F_{P1'} \cos\varphi_1 = F_{P2} \cos\varphi_1 + G_{z_21} - F_{C'1} \cos\varphi_1, \\ F_{C1} = F_{P1'} \sin\varphi_1 - F_{P2} \sin\varphi_1 + G_{x_21} + F_{C'1} \sin\varphi_1, \end{cases} \tag{9}$$

where

$$\begin{cases} G_{z_21} = m_1 g \cos\beta, \\ F_{C1} = -m_1 r_1 \left(\dfrac{v_1}{r_0}\right)^2 \operatorname{sgn}\dot{\theta}, \\ F_{C'1} = 0.5 m_1 l_1 \omega_1^2, \\ G_{x_21} = m_1 g \sin\beta \cos\theta. \end{cases} \tag{10}$$

From (4)–(6) and (9)–(10), it implies

$$\dot{\theta} = \frac{g \sin\beta \cos\theta + g \cos\beta \tan\varphi_1}{v_0}. \tag{11}$$

Rigid-body-1 rotates around o' in the $o'x_2z_2$ plane. According to the moment of momentum theorem, we have

$$\dot{M}_{m_1 v_1} = M_{F_{m_1}}, \tag{12}$$

where the moment of momentum $M_{m_1 v_1}$, the momentum M_1, and the resultant external moment $M_{F_{m_1}}$ are

$$\begin{cases} M_{m_1 v_1} = 0.5 M_1 l_1, \\ M_1 = m_1 v_1, \\ M_{F_{m_1}} = 0.5 F_{C1} l_1 \cos\varphi_1 + 0.5 G_{z_21} l_1 \cos\varphi_1 + 0.5 G_{z_20} l_1 \sin\varphi_1. \end{cases} \tag{13}$$

From (4), (9), (12)–(13), together with $v_1 = 0.5\omega_1 l_1$, it yields

$$\dot{\omega}_1 = \frac{1}{l_1}\left(-2v^2 \frac{1}{r_0} \cos\varphi_1 \operatorname{sgn}\dot{\theta} + 2g \sin\beta \cos\theta \cos\varphi_1 + 2g \cos\beta \sin\varphi_1 \right). \tag{14}$$

2.2.3 Force Analysis of m_3

Rigid-body-3 rotates around the hip joint in the $o'x_2z_2$ plane. Similar to (12), there exists

$$\dot{M}_{m_3 v_3} = M_{F_{m_3}}, \tag{15}$$

where the moment of momentum $M_{m_3v_3}$, the momentum M_3, and the resultant external moment of m_3 rotating around the hip joint $M_{F_{m_3}}$ are

$$\begin{cases} M_{m_3v_3} = M_3 l_3', \\ M_3 = m_3 v_3, \\ M_{F_{m_3}} = F_{C3}\ l_3' \cos\varphi_2 + G_{x_2 3} l_3' \cos\varphi_2 + G_{z_2 3} l_3' \sin\varphi_2, \end{cases} \tag{16}$$

with

$$\begin{cases} F_{C3} = -m_3 r_3 \left(\dfrac{v_3}{r_0}\right)^2 \operatorname{sgn}\dot{\theta}, \\ G_{x_2 3} = m_3 g \sin\beta\cos\theta, \\ G_{z_2 3} = m_3 g \cos\beta, \\ l_3' = 0.5 l_3 |\cos\varphi_4|. \end{cases} \tag{17}$$

From (3)–(5), (15)–(17), together with $v_3 = 0.5\omega_3 l_3$, we get

$$\dot{\omega}_3 = \frac{1}{l_3|\cos\varphi_4|}(T_1 + 2g\sin\beta\cos\theta\cos\varphi_3 + 2g\cos\beta) \tag{18}$$

with

$$T_1 = -2(v + l_2\omega_2\cos\varphi_2 + 0.5 l_3\omega_4\cos\varphi_4)^2 \cos\varphi_3 \frac{\operatorname{sgn}\dot{\theta}}{r_0}. \tag{19}$$

2.2.4 Force Analysis of the Overall System

Ignoring the relative displacement between the skier and the skis, the skier and the skis can be regarded as an overall system. Then, we analyze the forces applied to the overall system. As shown in Figure 7, according to Newton's Second Law, the following equation holds

$$F_N - G_{z_2} = m_1 a_{z_2 1} + m_2 a_{z_2 2} + m_3 a_{z_2 3}, \tag{20}$$

where $a_{z_2 1}$, $a_{z_2 2}$, and $a_{z_2 3}$ are the accelerations of m_1, m_2, and m_3 on $o'z_2$-axes, G_{z_2} is the gravity component of the overall system on $o'z_2$-axes with $G_{z_2} = (m_0 + m_1 + m_2 + m_3)g\cos\beta$. Since acceleration is the second derivative of displacement, it yields

$$\begin{cases} a_{z_2 1} = (0.5 l_1 \cos\varphi_1)'', \\ a_{z_2 2} = [(l_1 + 0.5 l_2 \cos\varphi_2)\cos\varphi_1]'', \\ a_{z_2 3} = [(l_1 + l_2\cos\varphi_2)\cos\varphi_1 + 0.5 l_3 \cos\varphi_3\cos\varphi_4]''. \end{cases} \tag{21}$$

In alpine skiing, there are some types of resistance, such as snow friction f_r and aerodynamic drag f_a. As shown in Figure 8, using Newton's Second Law again leads to

$$G_{y_2} - f_r - f_a = m_0 a_{y_2 0} + m_1 a_{y_2 1} + m_2 a_{y_2 2} + m_3 a_{y_2 3}, \tag{22}$$

where $a_{y_2 0}$, $a_{y_2 1}$, $a_{y_2 2}$, and $a_{y_2 3}$ are the accelerations of m_0, m_1, m_2, and m_3 on $o'y_2$-axes, G_{y_2} is the gravity component of the overall system on $o'y_2$-axes with $G_{y_2} = (m_0 + m_1 + m_2 +$

$m_3)g\sin\beta\sin\theta$. Moreover,

$$\begin{cases} f_r = \mu F_N, \\ f_a = 0.5 C_d \rho_a S v^2, \end{cases} \tag{23}$$

where μ is the dynamic coefficient of friction, S is the windward cross-sectional area of the skier, C_d is the drag coefficient, and ρ_a is the mass density of the air. Based on the real situation of skiing, the skier does not stay upright while skiing, and S changes with the skier's posture. According to the skier's posture, S can be written as

$$S = S_0 \frac{l_1 + l_2\cos\varphi_2 + l_3\cos\varphi_4}{l_1 + l_2 + l_3}, \tag{24}$$

where S_0 is the windward cross-sectional area of the skier when his body is upright. With the equations (2), (4), and (20)–(24), we get

$$\dot{v} = g\sin\beta\sin\theta + \frac{T_0 - f_r - f_a}{(m_0 + m_1 + m_2 + m_3)} \tag{25}$$

with

$$T_0 = (0.5 m_2 l_2 + m_3 l_2)(\omega_2^2 \sin\varphi_2 - \dot{\omega}_2 \cos\varphi_2) + 0.5 m_3 l_3 (\omega_4^2 \sin\varphi_4 - \dot{\omega}_4 \cos\varphi_4). \tag{26}$$

2.2.5 System Dynamic Equations

Consider the following system:

$$\dot{z} = f(z, u, t), \quad t_0 \le t \le t_f, \tag{27}$$

where the state $z = [x, y, \varphi_1, \varphi_2, \varphi_3, \varphi_4, \theta, v, \omega_1, \omega_2, \omega_3, \omega_4]^{\mathrm{T}} \in \mathbb{R}^{12}$, t_0 is the initial time of the system, and t_f is the final time of the system. Based on the real situation of skiing, the control variables $u = [u_1, u_2, u_3]^{\mathrm{T}} \in \mathbb{R}^3$ are defined as

$$\begin{cases} u_1 = \dfrac{1}{r_0}\operatorname{sgn}\dot{\theta}, \\ u_2 = \dot{\omega}_2, \\ u_3 = \dot{\omega}_4, \end{cases} \tag{28}$$

where the turning radius $r_0 = R_{SC}\cos\varphi$ with R_{SC} being the sidecut radius of skis. One may refer to [14] for the definition about R_{SC}. The control variable u_1 reflects the value of the turning radius. The control variables u_2 and u_3 are angular accelerations of the knee and hip joints, respectively, reflecting the strength of the knee and hip joints.

Based on the above derivations, we establish a skiing model that can describe the skier's

trajectory and posture simultaneously:

$$\begin{cases} \dot{x} = v\sin\theta, \\ \dot{y} = v\cos\theta, \\ \dot{\varphi}_1 = \omega_1, \\ \dot{\varphi}_2 = \omega_2, \\ \dot{\varphi}_3 = \omega_3, \\ \dot{\varphi}_4 = \omega_4, \\ \dot{\theta} = \dfrac{g\sin\beta\cos\theta + g\cos\beta\tan\varphi_1}{v}, \\ \dot{v} = g\sin\beta\sin\theta + \dfrac{T_0 - \mu F_N - f_a}{M}, \\ \dot{\omega}_1 = \dfrac{-2v^2u_1\cos\varphi_1 + 2g\sin\beta\cos\theta\cos\varphi_1 + 2g\cos\beta\sin\varphi_1}{l_1}, \\ \dot{\omega}_2 = u_2, \\ \dot{\omega}_3 = \dfrac{T_1 + 2g\sin\beta\cos\theta\cos\varphi_3 + 2g\cos\beta}{l_3|\cos\varphi_4|}, \\ \dot{\omega}_4 = u_3, \end{cases} \tag{29}$$

where

$$\begin{aligned} M &= m_0 + m_1 + m_2 + m_3, \\ T_0 &= (0.5m_2l_2 + m_3l_2)(\omega_2^2\sin\varphi_2 - u_3\cos\varphi_2) + 0.5m_3l_3(\omega_4^2\sin\varphi_4 - u_4\cos\varphi_4), \\ T_1 &= -2(v + l_2\omega_2\cos\varphi_2 + 0.5l_3\omega_4\cos\varphi_4)^2\cos\varphi_3u_1, \\ T_2 &= \omega_1^2\cos\varphi_1\cos\varphi_2 + \dot{\omega}_1\sin\varphi_1\cos\varphi_2 - 2\omega_1\omega_2\sin\varphi_1\sin\varphi_2 + \omega_2^2\cos\varphi_1\cos\varphi_2 \\ &\quad + \dot{\omega}_2\cos\varphi_1\sin\varphi_2, \\ T_3 &= \omega_3^2\cos\varphi_3\cos\varphi_4 + \dot{\omega}_3\sin\varphi_3\cos\varphi_4 - 2\omega_3\omega_4\sin\varphi_3\sin\varphi_4 + \omega_4^2\cos\varphi_3\cos\varphi_4 \\ &\quad + \dot{\omega}_4\cos\varphi_3\sin\varphi_4, \\ f_a &= 0.5C_d\rho_aS_0v^2\frac{l_1 + l_2\cos\varphi_2 + l_3\cos\varphi_4}{l_1 + l_2 + l_3}, \\ F_N &= Mg\cos\beta - l_2(0.5m_2 + m_3)T_2 - 0.5l_3m_3T_3 \\ &\quad - l_1(0.5m_1 + m_2 + m_3)(\omega_1^2\cos\varphi_1 + \dot{\omega}_1\sin\varphi_1). \end{aligned} \tag{30}$$

So far, we have established a skiing model based on force analysis. The skiing model can describe the skiers trajectory and posture simultaneously.

2.3 Model Stability Analysis

In alpine skiing, skiers need to tilt their bodies to adjust the turning radius. However, excessive tilting will lead to skiers tipping. It is crucial to ensure the stability of the human body during turning. Motivated by [15], this paper uses Zero-moment point (ZMP) theory to

carry out the stability analysis of the TRBP model. The ZMP is defined as the point at which the horizontal torque component of the ground force is zero. According to stability criterion of the ZMP theory, if the ZMP falls inside the convex polygon supported by the human body model, the model is stable and will not overturn. As shown in Figure 9, if the skier's ZMP falls inside the quadrilateral ABCD, the skier will not overturn.

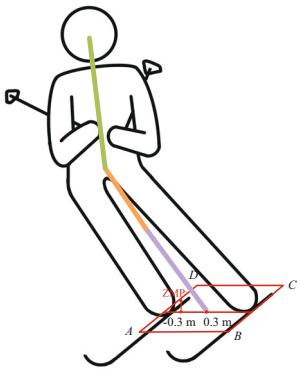

Figure 9 Schematic diagram of ZMP stability criterion for alpine skiing

Let $P(p_{x_2}, p_{y_2})$ denote the TRBP model's ZMP in the coordinates $o'x_2y_2z_2$. Motivated by [15], p_{x_2} can be expressed as

$$p_{x_2} = \frac{\sum_{i=1}^{n}(m_i(\ddot{z}_i + g)x_i - m_i(z_i - p_z)\ddot{x}_i)}{\sum_{i=1}^{n} m_i(\ddot{z}_i + g)}, \tag{31}$$

where n is the number of rigid bodies, m_i is the mass of rigid body i, x_i, y_i, and z_i are the coordinate values of rigid body i on the $o'x_2$, $o'y_2$ and $o'z_2$ axes, respectively. The procedure is complicated and we omit it for space.

When a skier skis, the skier is relatively stable in the sagittal plane ($o'y_2z_2$ plane). While, the movement range in the coronal plane ($o'x_2z_2$ plane) is extensive and the skier overturn easily. Thus, we only analyze the stability in the coronal plane of the human body. Considering the skier's posture in alpine skiing, the average distance between the feet is 0.6 m. According to ZMP stability criterion, the constraint of p_{x_2} is given by

$$-0.3 \leq p_{x_2} \leq 0.3. \tag{32}$$

Based on (31), together with (32), we derive the constraint condition of the three rigid bodies in the coronal plane as

$$-0.3 \leq \frac{\sum_{i=1}^{n}(m_i(\ddot{z}_i + g)x_i - m_i(z_i - p_z)\ddot{x}_i)}{\sum_{i=1}^{n} m_i(\ddot{z}_i + g)} \leq 0.3. \tag{33}$$

Thus far, we have derived an alpine skiing model (29) with the constraint condition (33). The establishment of the alpine skiing model is to optimize its trajectory and posture. The premise of optimization is to establish the optimization model which will be shown subsequently.

3 Optimization Model and Solving Method

In this section, we first use the alpine skiing models (29)–(30) to establish a multi-phase trajectory-and-posture optimization model. Then, we address the trajectory-and-posture optimization problem by using the well-known RPM.

3.1 Trajectory-and-Posture Optimization Model

We first describe the ski track information. As shown in Figure 10, there are red and blue alternating flag gates placed on the SG track. Skiers need to plan the skiing trajectory and pass through the flag gates correctly, otherwise the competition will fail. As shown in Figure 11, an SG gate consists of turning pole, turning gate, outside pole and outside gate.

Referring to the track design rules provided by the International Ski Federation (FIS), we design the SG track as shown in Figure 10. There are seven red and blue alternating flag gates on the track. The track has a slope of β and a length of 220 m.

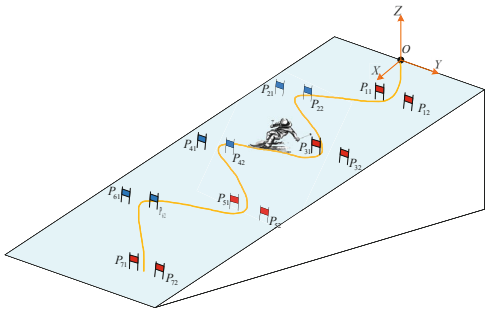

Figure 10 SG track

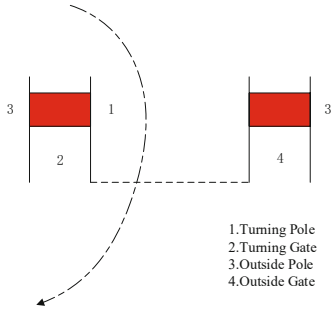

Figure 11 Schematic diagram of alpine ski flag gate setting

In $OXYZ$, the skiers' starting point O is $(0, 0)$. The coordinates of the k-th flag gate are $P_s^{(k)}(x_s^{(k)}, y_s^{(k)}, z_s^{(k)})$, where s represents the side of the flag gate, $k = 1, 2, \cdots, 7$, and $s = 1, 2$. The specific coordinates of each flag gate are shown in Table 2.

Table 2 Coordinates of the flag gates

Flag gate k	Left side ($s = 1$)	Right side ($s = 2$)
1	$P_1^{(1)}(30, 5, 0)$	$P_2^{(1)}(30, 12, 0)$
2	$P_1^{(2)}(55, -6, 0)$	$P_2^{(2)}(55, 0, 0)$
3	$P_1^{(3)}(85, 5, 0)$	$P_2^{(3)}(85, 11, 0)$
4	$P_1^{(4)}(115, -7, 0)$	$P_2^{(4)}(115.0, 0)$
5	$P_1^{(5)}(145, 4, 0)$	$P_2^{(5)}(145, 10, 0)$
6	$P_1^{(6)}(180, -7, 0)$	$P_2^{(6)}(180, -1, 0)$
7	$P_1^{(7)}(210, 5, 0)$	$P_2^{(7)}(210, 11, 0)$

Now, we establish the trajectory-and-posture optimization model. Considering that skiers have different constraints when passing through different flag gates, this paper transforms the

alpine skiing trajectory-and-posture optimization problem into a multi-phase optimal control problem. The first phase is from the initial point O to flag gate 1; the second phase is from flag gate 1 to flag gate 2, and so on. Let $t_0^{(k)}$ be the initial time of the k-th phase, $t_f^{(k)}$ be the final time of the k-th phase, $z_0^{(k)}$ be the initial state of the k-th phase, $z_f^{(k)}$ be the terminal state of the k-th phase, and $z^{(k)}$ be the general state of the k-th phase. Note that ${z_0}^{(k)} \in \mathbb{R}^{12}, {z_f}^{(k)} \in \mathbb{R}^{12}, z^{(k)} \in \mathbb{R}^{12}$, the initial, general, and terminal state of the k-th phase are denoted, respectively, by

$$
{z_0}^{(k)} = \left[{x_0}^{(k)}, {y_0}^{(k)}, {\varphi_{n0}}^{(k)}, {\theta_0}^{(k)}, {v_0}^{(k)}, {\omega_{n0}}^{(k)}\right]^{\mathrm{T}}, \tag{34}
$$

$$
{z_f}^{(k)} = \left[{x_f}^{(k)}, {y_f}^{(k)}, {\varphi_{nf}}^{(k)}, {\theta_f}^{(k)}, {v_f}^{(k)}, {\omega_{nf}}^{(k)}\right]^{\mathrm{T}}, \tag{35}
$$

$$
z^{(k)} = \left[x^{(k)}, y^{(k)}, {\varphi_n}^{(k)}, \theta^{(k)}, v^{(k)}, {\omega_n}^{(k)}\right]^{\mathrm{T}}, \tag{36}
$$

where $n = 1, 2, 3, 4$ and $k = 1, 2, \cdots, 7$.

Based on the skiing rules and the real skiing situations, the variables in the multi-phase are constrained as follows.

3.1.1 Initial Conditions

The initial conditions are

$$
\begin{cases}
{x_0}^{(1)} = 0 \text{ m}, \\
{y_0}^{(1)} = 0 \text{ m}, \\
{\varphi_{n0}}^{(1)} = 0 \text{ rad}, \\
{\theta_0}^{(1)} = \dfrac{\pi}{2} \text{ rad}, \\
{v_0}^{(1)} = 3 \text{ m/s}, \\
{\omega_{n0}}^{(1)} = 0 \text{ rad/s},
\end{cases} \tag{37}
$$

where $n = 1, 2, 3, 4$.

3.1.2 Path Constraints

Since skiers need to pass through the flag gate correctly, the path constraints are

$$
\begin{cases}
y_1^{(k)} \le y_f^{(k)} \le y_2^{(k)}, \\
x_1^{(k)} = x_f^{(k)} = x_2^{(k)},
\end{cases} \tag{38}
$$

where $k = 1, 2, \cdots, 7$.

3.1.3 Connection Conditions

The connection conditions for each phase are

$$
\begin{cases}
t_0^{(r+1)} = t_f^{(r)}, \\
z_0^{(r+1)} = z_f^{(r)},
\end{cases} \tag{39}
$$

where $r = 1, 2, \cdots, 6$.

3.1.4 Boundary Constraints

Based on the real skiing situations, the boundary constraints are given by

$$\begin{cases} 0 \text{ s} \le t_f^{(k)} \le 20 \text{ s}, \\ 0 \text{ m} \le x^{(k)} \le 220 \text{ m}, \\ -20 \text{ m} \le y^{(k)} \le 20 \text{ m}, \\ -\dfrac{7}{18}\pi \text{ rad} \le {\varphi_1}^{(k)} \le \dfrac{7}{18}\pi \text{ rad}, \\ 0 \text{ rad} \le {\varphi_2}^{(k)} \le \dfrac{1}{3}\pi \text{ rad}, \\ -\dfrac{7}{18}\pi \text{ rad} \le {\varphi_3}^{(k)} \le \dfrac{7}{18}\pi \text{ rad}, \\ -\dfrac{1}{3}\pi \text{ rad} \le {\varphi_4}^{(k)} \le 0 \text{ rad}, \\ 0 \text{ rad} \le \theta^{(k)} \le \pi \text{ rad}, \\ 3 \text{ m/s} \le v^{(k)} \le 50 \text{ m/s}, \\ -3.5 \text{ rad/s} \le {\omega_n}^{(k)} \le 3.5 \text{ rad/s}, \end{cases} \tag{40}$$

where $n = 1, 2, 3, 4$ and $k = 1, 2, \cdots, 7$.

In the SG, the athlete should pass through the flag gates correctly and take the shortest time over the specified course to win. Therefore, the control objective is to minimize the ski time and is expressed as

$$J = \sum_{k=1}^{7} J^{(k)} = \sum_{k=1}^{7} t_f^{(k)} - t_0^{(k)}, \tag{41}$$

where $J^{(k)}$ is the skiing time of the k-th phase.

3.2 Solution to Optimization Problem

This paper uses a direct numerical solution method to solve the multi-phase trajectory-and-posture optimization problem of the TRBP model. The direct method does not have the necessary conditions for the optimal solution, but discretized and parameterized the continuous optimal control problem, and searched the performance index directly by numerical method[16, 17]. The advantage of this method is that it can better compare the complex constraints, especially the path constraints[18]. The direct numerical solution method consists of two steps:

1) Discretizing the multi-phase continuous optimal control problem and transforming it into a nonlinear programming problem (NLP); and

2) solving the NLP problem with the SNOPT solver.

We use RPM to discretize the multi-phase continuous optimal control problem. RPM performs the pseudospectral transformation on continuous optimal problem in Legendre-Gauss-Radau (LGR) configuration points. It discretizes the state and control variables based on a global interpolation polynomial[19]. In recent years, RPM has been widely used in the aerospace and autonomous vehicle fields for trajectory optimization[20–28]. While, it is rarely used in

skiing. In this paper, we for the first time apply the RPM to solve trajectory-and-posture optimization problem for alpine skiing.

Consider the general form of the multi-phase optimal control problem:

$$J^{(k)} = \Phi^{(k)}\Big(z^{(k)}\Big(t_0^{(k)}\Big), t_0^{(k)}, z^{(k)}\Big(t_f^{(k)}\Big), t_f^{(k)}\Big) + \int_{t_0^{(k)}}^{t_f^{(k)}} g^{(k)}\big(z^{(k)}(t), u^{(k)}(t), t^{(k)}\big)dt, \tag{42}$$

$$\dot{z}^{(k)}(t) = f\big(z^{(k)}\big(t^{(k)}\big), u^{(k)}\big(t^{(k)}\big), t^{(k)}\big), \tag{43}$$

where k represents the k-th phase, $k = 1, 2, \cdots, K$, $J^{(k)}$ is the objective function of the k-th phase, $z^{(k)}$ is the state variable of the k-th phase, and $u^{(k)}$ is the control variable of the k-th phase. The discrete steps of the RPM for multi-phase optimal control problem are as follows.

First, the time interval $t \in \left[t_0^{(k)}, t_f^{(k)}\right]$ is mapped to the interval $\tau^{(k)} \in [-1, 1]$ via

$$\tau^{(k)} = \frac{2t}{t_f^{(k)} - t_0^{(k)}} - \frac{t_f^{(k)} + t_0^{(k)}}{t_f^{(k)} - t_0^{(k)}}. \tag{44}$$

Then, Lagrange interpolation is performed on $z^{(k)}$ and $u^{(k)}$, respectively, as

$$\begin{cases} z^{(k)}\left(\tau^{(k)}\right) \approx Z^{(k)}\left(\tau^{(k)}\right) = \displaystyle\sum_{j=1}^{N^{(k)}+1} L_j^{(k)}\left(\tau^{(k)}\right) Z_j^{(k)}, \\ u^{(k)}\left(\tau^{(k)}\right) \approx U^{(k)}\left(\tau^{(k)}\right) = \displaystyle\sum_{j=1}^{N^{(k)}} \widetilde{L}_j^{(k)}\left(\tau^{(k)}\right) U_j^{(k)}, \end{cases} \tag{45}$$

where $N^{(k)}$ is the number of LGR points in the k-th phase, $Z_j^{(k)} = Z^{(k)}\left(\tau_j^{(k)}\right)$, $U_j^{(k)} = U^{(k)}\left(\tau_j^{(k)}\right)$, $\tau_j^{(k)}$ is the time of the k-th phase at the j-th LGR point with $\tau_j^{(k)} \in [-1, 1)$, and $j = 1, 2, \cdots, N^{(k)}$. The Lagrange interpolation polynomials $L_i^{(k)}\left(\tau^{(k)}\right)$ and $\widetilde{L}_j^{(k)}\left(\tau^{(k)}\right)$ are defined as

$$\begin{cases} L_j^{(k)}(\tau^{(k)}) = \displaystyle\prod_{i=1, i\neq j}^{N^{(k)}+1} \frac{\tau^{(k)} - \tau_i^{(k)}}{\tau_j^{(k)} - \tau_i^{(k)}}, \\ \widetilde{L}_j^{(k)}(\tau^{(k)}) = \displaystyle\prod_{i=1, i\neq j}^{N^{(k)}} \frac{\tau^{(k)} - \tau_i^{(k)}}{\tau_j^{(k)} - \tau_i^{(k)}}, \end{cases} \tag{46}$$

where

$$L_j^{(k)}(\tau^{(k)}) = \begin{cases} 1, & i = j, \\ 0, & i \neq j, \end{cases} \tag{47}$$

$$\widetilde{L}_j^{(k)}(\tau^{(k)}) = \begin{cases} 1, & i = j, \\ 0, & i \neq j. \end{cases} \tag{48}$$

Taking the derivative of the first equation of (45) yields

$$\dot{Z}^{(k)}\big(\tau^{(k)}\big) = \sum_{j=1}^{N^{(k)}+1} \dot{L}_j^{(k)}\big(\tau^{(k)}\big) Z_j^{(k)}. \tag{49}$$

Based on the above derivations, the state function (43) and the objective function (42) approximated at LGR points are derived as

$$\sum_{j=1}^{N^{(k)}+1} D_{i,j}^{(k)} Z_j^{(k)} - \frac{t_f^{(k)} - t_0^{(k)}}{2} f^{(k)}\left(Z_i^{(k)}, U_i^{(k)}, \tau_i^{(k)}; t_0^{(k)}, t_f^{(k)}\right) = 0, \tag{50}$$

$$J = \sum_{k=1}^{K} \Phi^{(k)}\left(Z_0^{(k)}, \tau_0^{(k)}, Z_f^{(k)}, \tau_f^{(k)}\right) + \frac{t_f^{(k)} - t_0^{(k)}}{2} \sum_{k=1}^{K} \sum_{i=1}^{N^{(k)}} \omega_i^{(k)} g^{(k)}\left(Z_i^{(k)}, U_i^{(k)}, \tau_i^{(k)}; t_0^{(k)}, t_f^{(k)}\right), \tag{51}$$

where the pseudospectral differential matrix $D^{(k)} \in \mathbb{R}^{N^{(k)} \times (N^{(k)}+1)}$ with $D_{i,j}^{(k)} = \dot{L}_j^{(k)}\left(\tau^{(k)}\right)$, $i = 1, 2, \cdots, N^{(k)}$, $j = 1, 2, \cdots, N^{(k)} + 1$, and $\omega_i^{(k)}$ is the LGR weight in the k-th phase.

Through the above RPM transformation, the system dynamic equations (29)–(30) and objective function (42) are discretized and transformed into an NLP problem as

$$\begin{cases}
\sum\limits_{j=1}^{N^{(k)}+1} D_{ij}^{(k)} x_j^{(k)} = \dfrac{t_f^{(k)} - t_0^{(k)}}{2} v_i^{(k)} \sin\theta_i^{(k)}, \\
\sum\limits_{j=1}^{N^{(k)}+1} D_{ij}^{(k)} y_j^{(k)} = \dfrac{t_f^{(k)} - t_0^{(k)}}{2} v_i^{(k)} \cos\theta_i^{(k)}, \\
\sum\limits_{j=1}^{N^{(k)}+1} D_{ij}^{(k)} {\varphi_n}_j^{(k)} = \dfrac{t_f^{(k)} - t_0^{(k)}}{2} {\omega_n}_i^{(k)}, \\
\sum\limits_{j=1}^{N^{(k)}+1} D_{ij}^{(k)} \theta_j^{(k)} = \dfrac{t_f^{(k)} - t_0^{(k)}}{2} \dfrac{g\sin\beta\cos\theta_i^{(k)} + g\cos\beta\tan {\varphi_1}_i^{(k)}}{v_i^{(k)}}, \\
\sum\limits_{j=1}^{N^{(k)}+1} D_{ij}^{(k)} v_j^{(k)} = \dfrac{t_f^{(k)} - t_0^{(k)}}{2} \left[g\sin\beta\sin\theta_i^{(k)} + \dfrac{\widetilde{T}_0 - \mu\widetilde{F}_N - \widetilde{f}_a}{M}\right], \\
\sum\limits_{j=1}^{N^{(k)}+1} D_{ij}^{(k)} {\omega_1}_j^{(k)} = \dfrac{t_f^{(k)} - t_0^{(k)}}{2} \Big[-2(v_i^{(k)})^2 {u_1}_i^{(k)} \cos {\varphi_1}_i^{(k)} \\
\qquad\qquad +2g\sin\beta\cos\theta_i^{(k)} \cos {\varphi_1}_i^{(k)} + 2g\cos\beta\sin {\varphi_1}_i^{(k)}\Big], \\
\sum\limits_{j=1}^{N^{(k)}+1} D_{ij}^{(k)} {\omega_2}_j^{(k)} = \dfrac{t_f^{(k)} - t_0^{(k)}}{2} {u_2}_i^{(k)}, \\
\sum\limits_{j=1}^{N^{(k)}+1} D_{ij}^{(k)} {\omega_3}_j^{(k)} = \dfrac{t_f^{(k)} - t_0^{(k)}}{2} \cdot \dfrac{\widetilde{T}_1 + 2g\sin\beta\cos\theta_i^{(k)} \cos {\varphi_3}_i^{(k)} + 2g\cos\beta}{l_3 \left|\cos {\varphi_4}_i^{(k)}\right|}, \\
\sum\limits_{j=1}^{N^{(k)}+1} D_{ij}^{(k)} {\omega_4}_j^{(k)} = \dfrac{t_f^{(k)} - t_0^{(k)}}{2} {u_3}_i^{(k)},
\end{cases} \tag{52}$$

where $n = 1, 2, 3, 4$, the phase $k = 1, 2, \cdots, 7$, and

$$\begin{aligned}
\widetilde{T}_0 = {} & (0.5m_2l_2 + m_3l_2)\left[\left({\omega_2}_i^{(k)}\right)^2 \sin {\varphi_2}_i^{(k)} - {u_3}_i^{(k)} \cos {\varphi_2}_i^{(k)}\right] \\
& + 0.5m_3l_3\left[\left({\omega_4}_i^{(k)}\right)^2 \sin {\varphi_4}_i^{(k)} - {u_4}_i^{(k)} \cos {\varphi_4}_i^{(k)}\right],
\end{aligned}$$

$$\widetilde{T}_1 = -2\left(v_i^{(k)} + l_2\omega_{2i}^{(k)}\cos\varphi_{2i}^{(k)} + 0.5l_3\omega_{4i}^{(k)}\cos\varphi_{4i}^{(k)}\right)^2\cos\varphi_{3i}^{(k)}u_{1i}^{(k)},$$

$$\widetilde{T}_2 = \left(\omega_{1i}^{(k)}\right)^2\cos\varphi_{1i}^{(k)}\cos\varphi_{2i}^{(k)} + \left(\dot{\omega_1}_i^{(k)}\right)^2\sin\varphi_{1i}^{(k)}\cos\varphi_{2i}^{(k)} - 2\omega_{1i}^{(k)}\omega_{2i}^{(k)}\sin\varphi_{1i}^{(k)}\sin\varphi_{2i}^{(k)}$$
$$+ \left(\omega_{2i}^{(k)}\right)^2\cos\varphi_{1i}^{(k)}\cos\varphi_{2i}^{(k)} + u_{2i}^{(k)}\cos\varphi_{1i}^{(k)}\sin\varphi_{2i}^{(k)},$$

$$\widetilde{T}_3 = \left(\omega_{3i}^{(k)}\right)^2\cos\varphi_{3i}^{(k)}\cos\varphi_{4i}^{(k)} + \left(\dot{\omega_3}_i^{(k)}\right)^2\sin\varphi_{3i}^{(k)}\cos\varphi_{4i}^{(k)} - 2\omega_{3i}^{(k)}\omega_{4i}^{(k)}\sin\varphi_{3i}^{(k)}\sin\varphi_{4i}^{(k)}$$
$$+ \left(\omega_{4i}^{(k)}\right)^2\cos\varphi_{3i}^{(k)}\cos\varphi_{4i}^{(k)} + u_{3i}^{(k)}\cos\varphi_{3i}^{(k)}\sin\varphi_{4i}^{(k)},$$

$$\widetilde{f}_a = 0.5C_d\rho_a S_0\left(v_i^{(k)}\right)^2\frac{l_1 + l_2\cos\varphi_{2i}^{(k)} + l_3\cos\varphi_{4i}^{(k)}}{l_1 + l_2 + l_3},$$

$$\widetilde{F}_N = Mg\cos\beta - l_2(0.5m_2 + m_3)\widetilde{T}_2 - 0.5l_3m_3\widetilde{T}_3 - l_1(0.5m_1 + m_2 + m_3)$$
$$\cdot\left[\left(\omega_{1i}^{(k)}\right)^2\cos\varphi_{1i}^{(k)} + \sum_{j=1}^{N^{(k)}+1}D_{ij}^{(k)}\omega_{1j}^{(k)}\sin\varphi_{1i}^{(k)}\right], \tag{53}$$

$$J = \sum_{k=1}^{7}\sum_{i=1}^{N^{(k)}}\frac{t_f^{(k)} - t_0^{(k)}}{2}\omega_i^{(k)}. \tag{54}$$

Based on the equations (52)–(54), we can solve the NLP problem with the snopt solver in Matlab.

So far, we have established the multi-phase trajectory-and-posture optimization model and transformed it into an NLP problem by RPM method. Base on that, we can solve the multi-phase trajectory-and-posture optimization problem.

4 Simulation and Analysis

In this section, the simulation results under different parameters and control variables are obtained. The effects of body shape, minimum turning radius, and flexor and extensor strength of knees and hip joint are analyzed.

4.1 Simulation Results

Based on the multi-phase trajectory-and-posture optimization model (52)–(55), the stability constraint condition (33), and the state variables constraints (37)–(40), we solve the trajectory-and-posture optimization problem with the snopt solver in Matlab.

Considering the real skiing situation, the simulation parameter settings are as shown in Table 3 and the boundary constraints on control variables are given by

$$\begin{cases} -0.05 \le u_1 \le 0.05, \\ -2 \le u_2 \le 2, \\ -2 \le u_3 \le 2. \end{cases} \tag{55}$$

The trajectory, posture, and some kinematic parameters optimization results are obtained as follows.

Table 3 Simulation parameter values

Parameters	Notations	Value
Mass of skis (kg)	m_0	10
Mass of rigid-body-1 (kg)	m_1	10
Mass of rigid-body-2 (kg)	m_2	15
Mass of rigid-body-3 (kg)	m_3	50
Length of rigid-body-1 (m)	l_1	0.5
Length of rigid-body-2 (m)	l_2	0.45
Length of rigid-body-3 (m)	l_3	0.85
Acceleration of gravity (m/s^2)	g	9.8
The slope of the track ($\circ$)	β	20
Coefficient of friction	μ	0.04
Coefficient of aerodynamic drag	C_d	0.45
Air density (kg/m^3)	ρ_a	1.2
Windward area of the upright body (m^2)	S_0	0.4

4.1.1 Trajectory Optimization

The variables x and y are the skier's displacements on the OX-axis and OY-axis. We obtain the optimized displacements based on the snopt solver in Matlab and show the trajectory optimization result in Figure 12. The skier's center of gravity is always inclined to the inside of the turn, and the skier always tracks close to the steering gate when passing through the flag gate.

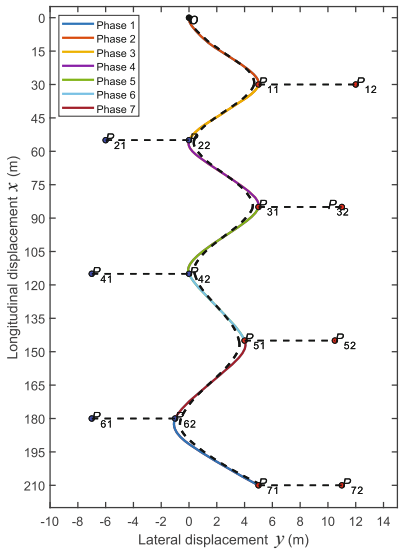

Figure 12 Multi-phase trajectory optimization results. The solid line indicates the optimal trajectory of the skier's skis, and the dashed line shows the optimal trajectory of the skier's center of gravity

4.1.2 Posture and Some Kinematic Parameters Optimization

Using the snopt solver in Matlab, we can not only solve for the skier's displacements based on the trajectory-and-posture optimization model (52)–(55), but also obtain the skier's posture and some kinematic parameters with the snopt solver. Figure 13 shows the changes of x, y, θ, v, φ_1, φ_2, φ_3, φ_4, and the height of the center of gravity G, respectively. As shown in Figure 13(e), the skier needs to tilt his lower limbs and increases the edge angle (φ_1) to reduce the turning radius when passing through the flag gate. It is worth noting that the angle of the skier's trunk (φ_3) is small. The skier need to keep his upper body almost upright to maintain his balance. In addition, the trunk and lower limbs of the skier are inclined in the same direction when turning.

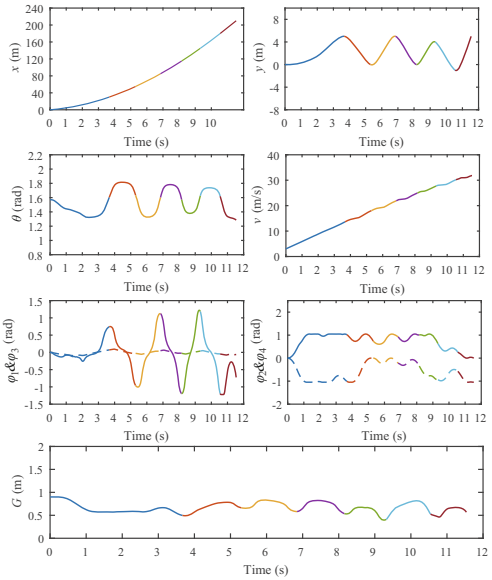

Figure 13 Results of multi-phase optimization of kinetic parameters: (a) Lateral displacement; (b) Longitudinal displacement; (c) Tangential angle; (d) Tangential velocity; (e) The tilt angle of the lower limbs φ_1 in the coronal plane (solid line) and the tilt angle of the trunk φ_3 in the coronal plane (dashed line); (f) The knees bending angle φ_2 (solid line) in the sagittal plane and the trunk bending angle φ_4 (dashed line) in the sagittal plane; and (g) Height of center of gravity

As shown in Figure 13(f), at the beginning of skiing, the skier needs to bend over (φ_4) and bend knees (φ_2) to reduce aerodynamic drag and increase velocity. When passing through the flag gate, the skier should straighten legs and bend over. Differently, the skier should bend legs and stretch the hip joint when he is in the middle of a phase.

Figure 13(g) shows the change of the skier's center of gravity. The skier lowers his center of gravity to reduce aerodynamic drag and increase velocity during the starting phase. The center of gravity drops to the lowest when passing through the flag gate. When the skier is in

the middle of a phase, the height of the center of gravity is raised.

4.1.3 Optimized Trajectory and Posture

The multi-phase trajectory-and-posture optimization model (52)–(55) can describe the skier's trajectory and posture simultaneously. To show the optimization results of trajectory and posture simultaneously, we display the optimized trajectory and posture on the three-dimensional ski track, as shown in Figure 14 (front, side, and vertical views). The green, orange, and purple lines represent the skier's trunk, thighs, and lower legs, respectively. It can be seen that the optimized trajectory and posture match the real skiing situation well.

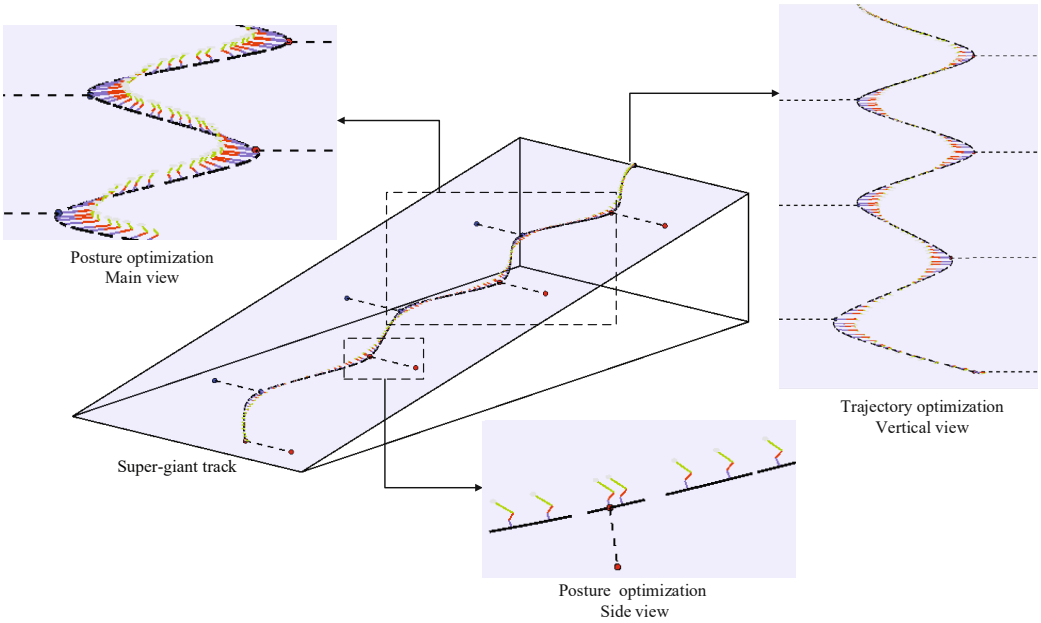

Figure 14 The optimized trajectory and posture diagram (front view, side view and verticle view)

4.2 Effect of Body Shape on Skiing Performance

The multi-phase trajectory-and-posture optimization model (52)–(55) can not only describe the skier's trajectory and posture, but also obtain the effect of different factors on skiing performance by comparing the optimization results under different model's parameters and control variables.

In competitive sports, the athlete's body shape is a key factor affecting sports performance. To explore the effect of skiers' body shape on skiing performance, we set different heights and weights of TRBP model with other parameters unchanged for simulation. The boundary constraints are given by (55). The trajectory, posture, and some kinematic parameters optimization results under different heights and weights are as follows.

4.2.1 Height

We obtain the optimization results for the height of TRBP model ranging from 1.5 m to 1.95 m with the weight being 75 kg. The effect of height on skiing time is shown in Figure 15.

It can been seen that the skiing time decreases as the height of the model increases. However, the time was only shortened by less than 0.1 s as the height increased from 1.5 m to 1.95 m. This indicates that the height is not significant in SG.

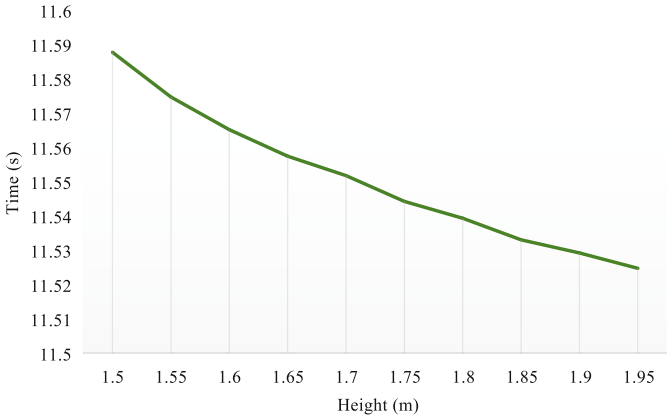

Figure 15 Effect of height on skiing time

Figure 16 and Figure 17 compare the skiing trajectory and posture optimization results for three heights (1.5 m, 1.8 m, and 1.95 m). It can be seen that the skiing trajectories (Figure 16) and curves of postural variables (Figure 17) for the different heights are close. Therefore, the skier's height has little effect on the skier's trajectory and posture.

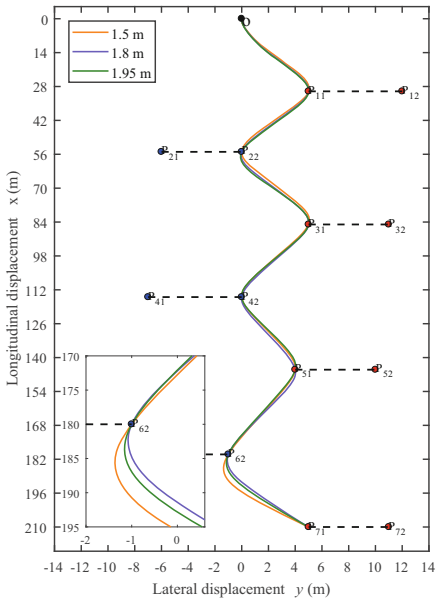

Figure 16 Skiing trajectory optimization results for three heights (1.5 m, 1.8 m, and 1.95 m)

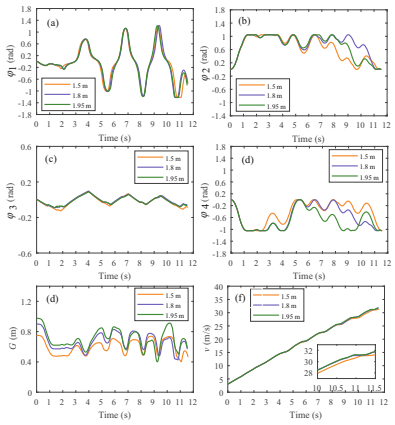

Figure 17 Skiing posture optimization results for three heights (1.5 m, 1.8 m, and 1.95 m): (a) The tilt angle of the lower limbs φ_1 in the coronal plane; (b) The tilt angle of the trunk φ_3 in the coronal plane; (c) The knees bending angle φ_2 in the sagittal plane; (d) The trunk bending angle φ_4 in the sagittal plane; (e) The height of the center of gravity; and (f) Tangential velocity

4.2.2 Weight

We obtain the optimization results for the weight of TRBP model ranging from 50 kg to 95 kg with the height being 1.8 m. The effect of weight on skiing time is shown in Figure 18. The result shows that the skiing time decreases as the model weight increases. It indicates that heavy skiers have an advantage in SG.

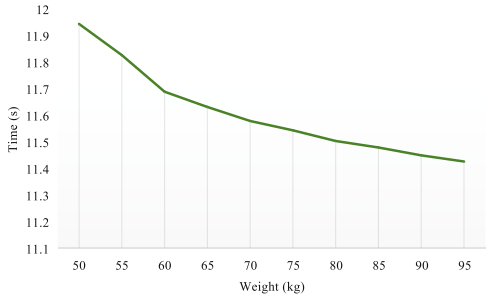

Figure 18 Effect of weight on skiing time

Figure 19 and Figure 20 compare skiing trajectory and posture optimization results for three weights (50 kg, 75 kg, and 95 kg). It can be seen that weight has a significant effect on skiing trajectory and posture. A heavier skier has larger angles of φ_1, φ_2, φ_3, and φ_4 when passing through the flag gate (Figure 20(a)–(d)). Moreover, Figure 20(e) and Figure 20(f) indicate that if the skier is heavier, his gravity center is lower and velocity is faster.

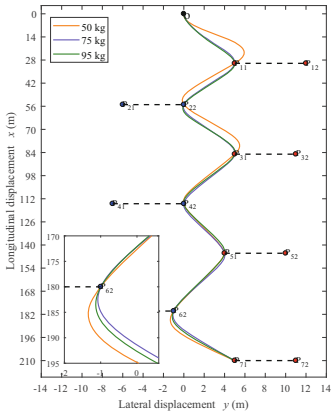

Figure 19 Skiing trajectory optimization results for three weights (50 kg, 75 kg, and 95 kg)

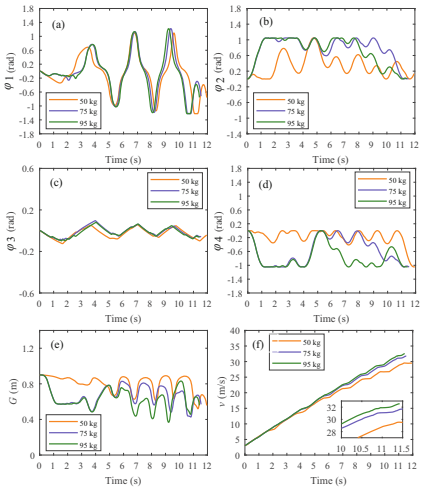

Figure 20 Skiing posture optimization results for three weights (50 kg, 75 kg, and 95 kg): (a) The tilt angle of the lower limbs φ_1 in the coronal plane; (b) the tilt angle of the trunk φ_3 in the coronal plane; (c) the knees bending angle φ_2 in the sagittal plane; (d) the trunk bending angle φ_4 in the sagittal plane; (e) the height of center of gravity; and (f) tangential velocity

4.3 Effect of the Minimum Turning Radius on Skiing Performance

The minimum turning radius is defined as the smallest radius when the skier carves in a ski turn. The minimum radius is different for skiers with different technical characteristics, physical fitness, and athletic ability. To show the effect of the minimum turning radius on skiing performance, we set the minimum turning radius from 13 m to 26 m for simulation while holding other parameters unchanged.

According to (28), the value range of u_1 is related to the value range of the turning radius, and

$$u_{1\max} = \frac{1}{r_{0\min}} \operatorname{sgn} \dot{\theta}, \tag{56}$$

where $u_{1\max}$ is the maximum value of u_1 and $r_{0\min}$ is the minimum turning radius. We set $0.0385 \leq u_{1\max} \leq 0.0769$ with $-2 \leq u_2 \leq 2$ and $-2 \leq u_3 \leq 2$. The weight and height of TRBP model are set as 75 kg and 1.8 m, respectively.

Figure 21 shows the effect of $r_{0\min}$ on skiing time. As $r_{0\min}$ becomes smaller, its effect on skiing performance becomes weaker. Therefore, a small turning radius is conducive to getting good skiing performance.

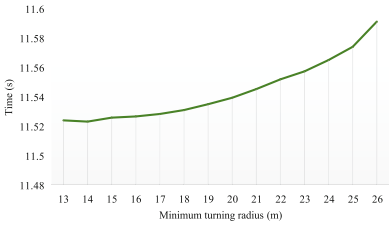

Figure 21 Effect of the minimum turning radius on skiing time

Figure 22 and Figure 23 show the skiing trajectory optimization results under three different $r_{0\min}$. As shown in Figure 22, when passing through the flag gate, the skiers with a smaller $r_{0\min}$ are closer to the turning gate. In addition, Figure 23(a) and Figure 23(c) show that the skier with a greater swing of the lower limbs and a more stable upper body performs better. Moreover, the change of $r_{0\min}$ has little effect on the skiing velocity (Figure 23(f)).

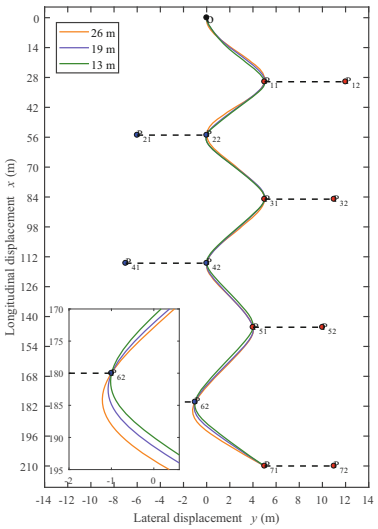

Figure 22 Skiing trajectory optimization results under three different $r_{0\min}$ (26 m, 19 m, and 13 m)

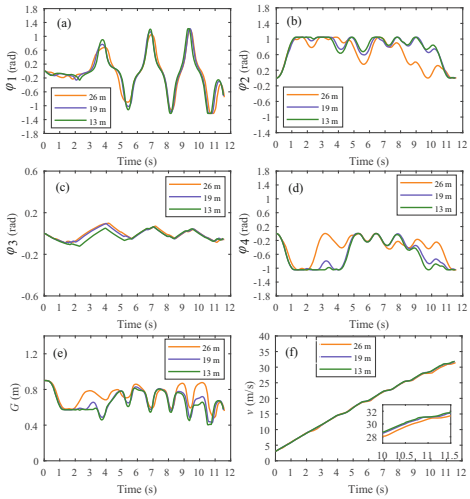

Figure 23 Skiing posture optimization results under three different $r_{0\,\min}$ (26 m, 19 m, and 13 m): (a) The tilt angle of the lower limbs φ_1 in the coronal plane; (b) The tilt angle of the trunk φ_3 in the coronal plane; (c) The knees bending angle φ_2 in the sagittal plane; (d) The trunk bending angle φ_4 in the sagittal plane; (e) The height of center of gravity; and (f) Tangential velocity

4.4 Effect of Knees and Hip Joint Flexor and Extensor Strength

According to the law of rotation $M = J\dot{\omega}$, the angular acceleration $\dot{\omega}$ of fixed axis rotation of a rigid body is directly proportional to its external torque M and inversely proportional to its moment of inertia J. Therefore, the greater angular acceleration represents the greater force on the revolute joint with the same moment of inertia. The angular acceleration of the knee joints $\dot{\omega}_2$ indicates the flexor and extensor strength of the knee joints. The larger the value of $\dot{\omega}_2$ is, the greater the force of the knee joints is. Similarly, the angular acceleration between the thighs and trunk $\dot{\omega}_4$ indicates the flexor and extensor strength of the hip joint. The larger the $\dot{\omega}_4$ is, the greater the force of the hip joint is.

To show the effect of knees and hip flexor and extensor strength on skiing performance, we change the range of $\dot{\omega}_2$ and $\dot{\omega}_4$ with other parameters being unchanged. According to (29), $u_2 = \dot{\omega}_2$ and $u_3 = \dot{\omega}_4$. We set $u_{2\,\max}$ from 2 ω/s^2 to 5 ω/s^2 and $u_{3\,\max}$ from 1.5 ω/s^2 to 5 ω/s^2, respectively, with $-0.05 \leq u_1 \leq 0.05$. The weight and height of TRBP model are set as 75 kg and 1.8 m, respectively.

The optimization results under different $u_{2\,\max}$ and $u_{3\,\max}$ are shown in Figure 24. The skiing time decreases when the angular accelerations of flexion and extension of the knees ($u_{2\,\max}$) and hip joint ($u_{3\,\max}$) increase.

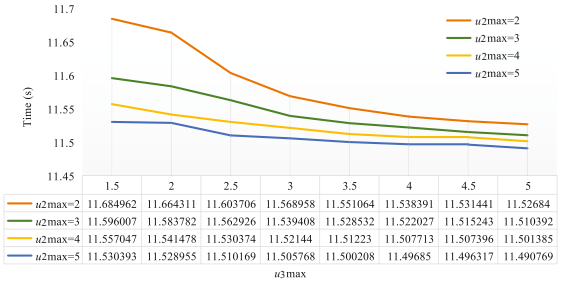

	1.5	2	2.5	3	3.5	4	4.5	5
u2max=2	11.684962	11.664311	11.603706	11.568958	11.551064	11.538391	11.531441	11.52684
u2max=3	11.596007	11.583782	11.562926	11.539408	11.528532	11.522027	11.515243	11.510392
u2max=4	11.557047	11.541478	11.530374	11.52144	11.51223	11.507713	11.507396	11.501385
u2max=5	11.530393	11.528955	11.510169	11.505768	11.500208	11.49685	11.496317	11.490769

u3max

Figure 24 Effect of flexor and extensor strength of the knees and hip joint on skiing performance

According to the reference [29], knee flexion is related to the biceps femoris, semitendinosus, semimembranosus, sartorius, gracilis, and gastrocnemius, while extension is related to the quadriceps femoris. Hip flexion is associated with the iliopsoas and rectus femoris muscles, while extension is associated with the gluteus maximus and biceps femoris. Athletes can boost the training of the related muscle groups to increase the flexor and extensor strength of the knees and hip joint to control posture and improve skiing performance better.

So far, we have showed the optimization results of TRBP model under different parameters and control variables, based on which the effects of body shape, the minimum turning radius, and the flexor and extensor strength of knees and hip joint on skiing performance are analyzed. Through simulations, we can see that the TRBP model can represent the skier's trajectory and posture simultaneously, which can not be achieved by existing models.

5 Conclusions

This paper has established a TRBP model which can represent skiers trajectory and posture characteristics simultaneously. Simulation results have verified the effectiveness of the proposed model and obtained optimal skiing trajectory, skiing posture, and some key kinematic parameters of skier. By analyzing the effects of different body shapes, minimum turning radius, and flexor and extensor strength of knees and hip joint on skiing performance, the following conclusions are drawn:

1) Tall and heavy skiers have advantages in skiing, but height has little effect on skiing performance while weight significantly impacts skiing performance.

2) The skier with a smaller turning radius can have a closer trajectory to the turning gate and shorter skiing time.

3) Strengthening the knees and hip joint can improve the skier's posture control to reduce skiing time.

Based on the conclusions, we provide the following advice for skiers and coaches:

1) Appropriately increasing the skier's weight can improve skiing performance.

2) On the basis of keeping the body stable, increasing the lower limb tilt angle in the coronal plane can reduce the turning radius and make the skiing trajectory closer to the steering gate, so as to shorten the skiing time.

3) Skiers should keep their trunk upright when passing through the flag gate, which helps to ensure body stability and prevent rollover.

4) Skiers can strengthen the training of the muscle groups related to the knees and hip joint to control body posture better and improve skiing performance.

For skiers, we provide guidance for their training with the help of scientific technology. The skiers can capture their ski trajectories and postures with detection sensors and compare these real information with our optimized skiing trajectory and posture, based on which they can improve skiing performance. Coaches can analyze the trajectories and postures of skiers based on the optimization results, and then specify scientifically personalized training plans for skiers. For skiing researchers, our established TRBP model provides a basis for subsequent skiing research. In the future, we aim to establish a model that more closely resembles the real alpine skiing system and consider more details such as changes in terrain and changes in ski geometry.

Conflict of Interest

SUN Jian is an editorial board member and ZHANG Yanjun is a youth editorial board for Journal of System Science & Complexity and was not involved in the editorial review or the decision to publish this article. All authors declare that there are no competing interests.

References

[1] Natalia B, Carlota T, Robert H, et al., Overview of complex systems in sport, *Journal of Systems Science & Complexity*, 2013, **26**(1): 4–13.

[2] Julian M J, Mora A M, and Carlos C, Complex systems in sports: Introduction to the special issue, *Journal of Systems Science & Complexity*, 2013, **26**(1): 1–3.

[3] Sung D J, Park S J, Kim S, et al., Effects of core and non-dominant arm strength training on drive distance in elite golfers, *Journal of Sport and Health Science*, 2016, **5**(2): 219–225.

[4] Malte S and Martin L, Modeling soccer by means of relative phase, *Journal of Systems Science & Complexity*, 2013, **26**(1): 14–20.

[5] Allinger T L and Bogert A, Skating technique for the straights, based on the optimization of a simulation model, *Med. Sci. Sports Exerc.*, 1997, **29**(2): 279–286.

[6] Cai C and Yao X, Trajectory optimization with constraints for alpine skiers based on multi-phase nonlinear optimal control, *Frontiers of Information Technology & Electronic Engineering*, 2020, **521**(10): 1521–1534.

[7] Legotin S D, Obnosov K B, and Rivlin A A, Mechanics of alpine skiing: Carve turn with angulation, *Journal of Physics: Conference Series*, 2020, **1705**(1): 12034–12046.

[8] Komissarov S S, Dynamics of carving runs in alpine skiing, The basic centrifugal pendulum, *Sports Biomechanics*, 2022, **21**(8): 890–911.

[9] Cai C and Yao X, Dynamic analysis and trajectory optimization for the nonlinear ski-skier system, *Control Engineering Practice*, 2021, **114**(1): 104868.

[10] Morawski J M, Control systems approach to a ski-turn analysis, *Journal of Biomechanics*, 1973, **6**(3): 267–279.

[11] Rudakov R, Lisovski, Ilyalov O, et al., Optimisation of the skiers trajectory in special slalom, *Procedia Engineering*, 2020, **2**(2): 3179–3182.

[12] Sundstrm D, Carlsson P, Sthl F, et al., Numerical optimization of pacing strategy in cross-country skiing, *Structural and Multidisciplinary Optimization*, 2013, **47**(6): 943–950.

[13] Sun Y, Guo R, Gao L, et al., Research on the inrun profile optimization of ski jumping based on dynamics, *Structural and Multidisciplinary Optimization*, 2021, **63**(3): 1481–1490.

[14] Hubisz J L, The physics of skiing: Skiing at the triple point, *The Physics Teacher*, 2004, **42**(5): 318–318.

[15] Erbatur K, Okazaki A, Obiya K, et al., A study on the zero moment point measurement for biped walking robots, 7*th International Workshop on Advanced Motion Control*, Maribor, 2002, 431–436.

[16] Ma B, A singular linear quadratic time-iInconsistent optimal control problem, *Journal of Systems Science & Complexity*, 2023, **36**(3): 1024–1052.

[17] Liu J, Wang Y, and Zhang N, Optimal reinsurance and dividend under model uncertainty, *Journal of Systems Science & Complexity*, 2023, **36**(3): 1116–1143.

[18] Wang D, Pan Q, Hu J, et al., Nonlinear model predictive control for trajectory tracking of quadrotors using Lyapunov techniques, *Science China Information Sciences*, 2022, **65**: 1–2.

[19] Li J, Fuel-optimal low-thrust formation reconfiguration via Radau pseudospectral method, *Advances in Space Research*, 2016, **58**(1): 1–16.

[20] Ross I M and Karpenko M, A review of pseudospectral optimal control: From theory to flight, *Annual Reviews in Control*, 2012, **36**(2): 182–197.

[21] Garg D, Patterson M, Hager W W, et al., A unified framework for the numerical solution of optimal control problems using pseudospectral methods, *Automatica*, 2020, **46**(11): 1843–1851.

[22] Garg D, Hager W W, and Rao A V, Pseudospectral methods for solving infinite-horizon optimal control problems, *Automatica*, 2011, **47**(4): 829–837.

[23] Huntington G T and Rao A V, Optimal reconfiguration of spacecraft formations using the Gauss pseudospectral method, *Journal of Guidance Control & Dynamics*, 2012, **31**(3): 689–698.

[24] Han F, Wang Z, He L, et al., Trajectory plan for an ultra-short distance on-orbit service based on the Gaussian pseudo-spectral method, *IEEE/CAA Journal of Automatica Sinica*, 2018, 1–9, DOI: 10.1109/JAS2017.7510892.

[25] Jorris T R and Cobb R G, Three-dimensional trajectory optimization satisfying waypoint and no-fly zone constraints, *Journal of Guidance, Control, and Dynamics*, 2009, **32**(2): 551–572.

[26] Wu B, Qian L, Lu M, et al. Optimal control problem of multi-vehicle cooperative autonomous parking trajectory planning in a connected vehicle environment, *IET Intelligent Transport Systems*, 2020, **13**(1): 1677–1685.

[27] Wang D, Wang Z, Wu Z, et al., Distributed convex optimization for nonlinear multi-agent systems disturbed by a second-order stationary process over a digraph, *Science China Information Sciences*, 2022, **65**(3): 132201.

[28] Zhou Z, Liu Z, Su H, et al., Multi-objective optimization for 10-kW rated power dynamic wireless charging systems of electric vehicles, *Science China Information Sciences*, 2022, **65**(10): 202201.

[29] Delp S L, Loan J P, Hoy M J, et al., An interactive graphics-based model of the lower extremity to study orthopaedic surgical procedures, *IEEE Transactions on Biomedical Engineering*, 1990, **37**(8): 757–767.